

Nanoscale laminin coating modulates cortical scarring response around implanted silicon microelectrode arrays

Wei He¹, George C McConnell¹ and Ravi V Bellamkonda

Neurological Biomaterials and Therapeutics, Wallace H Coulter Department of Biomedical Engineering, Georgia Institute of Technology/Emory University, 313 Ferst Drive, Atlanta, GA 30332, USA

E-mail: ravi@bme.gatech.edu

Received 29 August 2006

Accepted for publication 25 October 2006

Published 15 November 2006

Online at stacks.iop.org/JNE/3/316

Abstract

Neural electrodes could significantly enhance the quality of life for patients with sensory and/or motor deficits as well as improve our understanding of brain functions. However, long-term electrical connectivity between neural tissue and recording sites is compromised by the development of astroglial scar around the recording probes. In this study we investigate the effect of a nanoscale laminin (LN) coating on Si-based neural probes on chronic cortical tissue reaction in a rat model. Tissue reaction was evaluated after 1 day, 1 week, and 4 weeks post-implant for coated and uncoated probes using immunohistochemical techniques to evaluate activated microglia/macrophages (ED-1), astrocytes (GFAP) and neurons (NeuN). The coating did not have an observable effect on neuronal density or proximity to the electrode surface. However, the response of microglia/macrophages and astrocytes was altered by the coating. One day post-implant, we observed an ~60% increase in ED-1 expression near LN-coated probe sites compared with control uncoated probe sites. Four weeks post-implant, we observed an ~20% reduction in ED-1 expression along with an ~50% reduction in GFAP expression at coated relative to uncoated probe sites. These results suggest that LN has a stimulatory effect on early microglia activation, accelerating the phagocytic function of these cells. This hypothesis is further supported by the increased mRNA expression of several pro-inflammatory cytokines (TNF- α , IL-1 and IL-6) in cultured microglia on LN-bound Si substrates. LN immunostaining of coated probes immediately after insertion and retrieval demonstrates that the coating integrity is not compromised by the shear force during insertion. We speculate, based on these encouraging results, that LN coating of Si neural probes could potentially improve chronic neural recordings through dispersion of the astroglial scar.

(Some figures in this article are in colour only in the electronic version)

Abbreviations

Si	silicon
PEI	polyethyleneimine
LN	laminin
LbL	layer-by-layer
MEA	multielectrode array
GFAP	glial fibrillary acid protein

CNS	central nervous system
IL-1	interleukin-1
IL-6	interleukin-6
TNF- α	tumor necrosis factor α

1. Introduction

Neural interface technology holds the exciting potential of allowing direct communication between nervous tissue and

¹ These authors contributed equally.

external electronics. This technology has already significantly enhanced the quality of life for many patients with sensory and/or motor deficits as is evident from both the prosthetic cochlear implant, commonly used for treatment of deafness [1, 2], and deep brain stimulation, which has been used to reduce motor symptoms associated with Parkinson's Disease [3–5]. Silicon microelectrode arrays (Si MEAs) have been a driving force in the advancement of neural interface technology with several advantages over competitive devices including high-density recording sites, batch fabrication, highly reproducible geometry and user-customizable dimensions [6]. These micromachined neural prosthetic devices have been used to stimulate and record from the central and peripheral nervous systems [7–10]. In order to further advance the clinical applications for silicon microelectrode technology, several issues need to be addressed, one of which is improving the reliability of long-term recordings from single units [11]. The underpinning reason for the unreliability is still being investigated. One speculated cause is adverse tissue response induced by the implant. Therefore, the effectiveness of these neural implants could decrease with time following their implantation, either due to implant-induced astrogliosis, a process which electrically and mechanically isolates the prosthesis from the nervous system [12, 13], and/or due to neuronal cell loss surrounding these devices [14, 15].

Considering that neural interfaces must meet strict demands on long-term performance for clinical efficacy, several strategies have been undertaken to improve the biocompatibility of these devices [16]. One approach to improve the neuron-implant interface is to coat the microelectrode surface with molecules which promote tissue integration [17–20]. We have previously reported an ultrathin coating of laminin-1 (LN) on Si/SiO₂ surfaces using surface modification by electrostatic layer-by-layer (LbL) self-assembly [21]. The advantage of this technique is its versatility and fine control over layer thickness, which has ramifications on both the stability and impedance characteristics of the coatings. As shown in the previous work, the impedance magnitude at 1 kHz for the coating-modified microelectrode was not statistically different from bare microelectrodes.

The biological contribution to degradation in recording quality over the duration of an implant is currently unknown. Neuronal-related hypotheses generally relate to the physical distance between neurons and recording sites being increased. This may be due to glial cells pushing neurons away and/or neuronal death in the immediate vicinity of the electrode. It has also been suggested that the glial cellular response plays a critical part in recording quality by increasing electrode impedance and creating shunt pathways for current to travel away from recording sites [22].

In this study, we investigate the cortical response, including glial and neuronal cells, to chronically implanted coated Si MEAs compared to uncoated controls in a rat model. We demonstrate that ultrathin LN coatings significantly decrease chronic immunoreactivity, specifically, the gliosis response around coated probes after 4 weeks compared to uncoated bare Si probes.

2. Materials and methods

2.1. Preparation of nanoscale LN coatings by LbL

Polyethyleneimine (PEI, Aldrich, MW 25,000) was dissolved in Ultrapure water (MilliQ-plus system, Millipore) with a resistivity of 18.2 M Ω cm to a final concentration of 3 mg ml⁻¹ and pH adjusted to 7.4. The solution was then sterilized by filtration through a 0.2 μ m sterile filter in a laminar flow hood. Laminin-1 (LN) was purchased from BD Bioscience and diluted to a concentration of 0.2 mg ml⁻¹ with phosphate buffered saline (PBS) solution at pH 7.4. Single shank neural probes were obtained from NeuroNexus Technologies. Shank dimensions were 5 mm in length, 33–200 μ m wide and 15 μ m thick.

LbL surface coatings on the neural probes were prepared according to the method described previously [21]. Briefly, a PEI layer was adsorbed for 30 min onto the neural probes as a precursor layer to initiate the LbL self-assembly. The build-up of the multilayer was accomplished by consecutive adsorption of the oppositely charged polycations PEI and polyanions LN onto the probes. Between each step, the excess polyelectrolyte was removed by rinsing the sample surface with sterile water. For each layer, an incubation time of 20 min and a rinsing time of 1 min were used. A total of eight bilayers of PEI-LN were built on the neural probes.

2.2. Evaluation of surface structure and coating integrity

Scanning electron microscopy (SEM) was performed on probes with or without the coating. Images were taken using a LEO 1530 thermally-assisted field emission (TFE) scanning electron microscope at a 5 kV accelerating voltage. In order to determine whether the insertion procedure disrupts the coating integrity, coated probes ($n = 4$) were inserted into a PBS-perfused rat brain, and subsequently retrieved. The retrieved probes were stained for LN using primary antibody rabbit anti-LN (1:500; Sigma) and secondary antibody goat anti-rabbit IgG Alexa 594 (1:220; Molecular Probes).

2.3. Surgical procedures for chronic implants

Animal procedures adhered to the National Institute of Health (NIH) guidelines and followed a protocol approved by the Institutional Animal Care and Use Committee (IACUC) at Georgia Institute of Technology. Adult male Sprague-Dawley rats were used in this study. This animal model is relevant for the study of chronic tissue reaction to cortical implants, as the glial response has been reported to be similar between rat and non-human primate models [22]. Adult male rats (275–299 g) were anesthetized for 5 min with a mixture of 5% isoflurane and 1 L min⁻¹ O₂ prior to surgery. Each animal was positioned into a stereotactic frame (Kopf) where anesthesia was maintained at 2–3% isoflurane during surgery (with 0.3 L min⁻¹ O₂). The animal's head was shaven over the incision area and the skin was disinfected with isopropyl alcohol and chlorohexaderm using a scrubbing motion before making the incision. Ophthalmic ointment was applied to the eyes to prevent drying. A midline incision was made

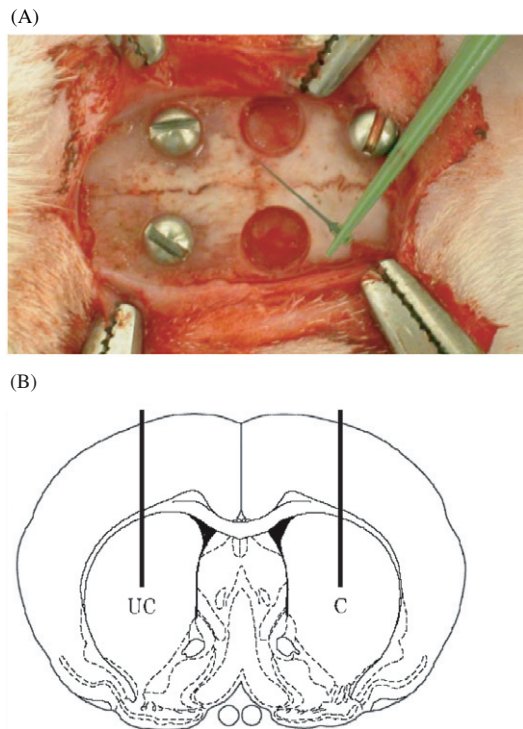


Figure 1. (A) Micrograph of surgical field-of-view prior to inserting probes. Background: two craniotomy sites and three stainless-steel bone screws. Foreground: probe grabbed with Teflon coated microforceps. (B) Schematic of insertion locations for uncoated (UC) and coated (C) probes (+0.2 mm Bregma, ± 3 mm Lateral). Two vertical lines represent probes inserted through the cortex and striatum. Coronal section of adult rat brain adapted from Paxinos and Watson [23].

along the scalp, the skin retracted, and the periosteum cleared to expose the bregma. A dental drill was used to create a 3.2 mm hole at +0.2 mm anterior and +3.0 mm lateral to the bregma with a custom trephine (24 tooth \times 3 mm O.D.) fabricated from stainless steel tubing (Small Parts). In order to minimize iatrogenic damage, room temperature saline was applied liberally to the spinning drill bit at the bone interface. The bone plug was carefully removed and the dura was gently pierced and retracted with fine microforceps. The bond-pad region of the coated microelectrode was grasped with Teflon-coated microforceps and the penetrating shank was inserted by hand through the pia into the cortex (figure 1(A)). Electrode insertion by hand, used in this study, was shown by the previous work [12] to make little difference in tissue reaction around the electrode compared to the automated insertion method. The probe was inserted to the point where only the bond-pad region was visible outside the cortical surface. A craniotomy of identical diameter was made over the contralateral location (+0.2 mm anterior to the Bregma and -3.0 mm lateral to the midline suture) where the control probe was inserted the same way as described above (figure 1(B)). Variations were minimized between rats by having both the control and treated probes within the same animal. Variations in insertion depth

between the two hemispheres were minimized by inserting the shanks up to the bond-pad, as opposed to estimating a more shallow insertion. After insertion, the bond-pad regions of the probes and the holes were covered with 1% SeaKem[®] Agarose (Cambrex) gel. The craniotomy was further sealed using dental acrylic anchored to the skull using bone screws (Plastics One, Inc.). The skin was sutured shut with 4-0 monofilament nylon and the animals were monitored carefully until full recovery.

2.4. Brain tissue preparation for immunohistochemistry

Animals were prepared for immunohistochemistry 1 day, 1 week and 4 weeks after device insertion ($n = 3$ animals per time point). Each animal was anesthetized with a mixture of ketamine (45.65 mg kg^{-1}), xylazine (9.13 mg kg^{-1}) and acepromazine (1.52 mg kg^{-1}). Animals were then perfused intracardially with PBS prewash followed by 4% paraformaldehyde in PBS. The brains were removed and postfixed for 24 h (4 °C). The implanted neural probes were then carefully pulled out of the tissue and the brains were placed into 30% sucrose (4 °C) until they sank to the bottom. The brains were then cryoprotected with optimal cutting temperature (OCT) compound (Tissue-Tek). In order to differentiate between hemispheres, tissue dye was applied to one hemisphere posterior to the insertion sites. Horizontal 30 μm thick tissue sections were cut through the cortex of all brains and the sections were stored at 4 °C in PBS with 0.01% sodium azide. While the recording sites were located below the cortex, probe width decreases toward the tip (the location of the recording sites). It was therefore assumed that cortical tissue reaction would be overestimated in comparison to the case where recording sites are located in the cortex.

2.5. Immunohistochemistry

To study brain tissue response in the cortical region, cortical sections taken from all brains from each group were stained simultaneously for the antibody of interest. Sections were blocked in 4% normal goat serum (GIBCO) with PBS containing 0.5% Triton X-100 (Sigma) for 1 h at room temperature. Sections were then immediately incubated overnight at 4 °C with primary antibody prepared in blocking solution. Antibodies for the following molecules were used: ED-1 (marker of reactive microglia and macrophages; CD 68 monoclonal mouse IgG1, 1:1000; Serotec); GFAP (specific to astrocytes; polyclonal rabbit IgG, 1:2000; Dako); NeuN (specific to neurons; mouse IgG1, 1:500; Chemicon). After washing in 0.5% triton in PBS, sections were incubated in secondary antibodies for 1 h at room temperature. Secondary antibodies were diluted at a ratio of 1:220 in 0.5% triton in PBS, and included goat anti-rabbit IgG (H + L) Alexa 594 (Molecular Probes) and goat anti-mouse IgG1 Alexa 488 (Molecular Probes). All sections were counterstained by incubation with the nuclear dye DAPI (Molecular Probes) that labeled cell nuclei. Tissue sections were mounted on glass microscope slides with Fluoromount-G (Southern Biotechnology Associates).

2.6. Quantitative analysis of immunohistochemical data

All fluorescent images were acquired using a Microfire digital camera and a Zeiss Axioskop2 Plus upright microscope, with the probe site centered in the camera field. In order to minimize unequal illumination, all the images for each marker of interest, i.e. ED-1, GFAP and NeuN, were collected under the same exposure settings within the same day. Image analysis was performed using custom software developed in MATLAB (Image Processing Toolbox included). GFAP intensity as a function of distance from the probe–tissue interface was calculated based on a method used previously [24]. An example is given in figure 2(A). For each image a point was manually selected within the probe site and an edge detection algorithm was used to locate the probe–tissue interface (zero-crossing method). This functioned as the zero point for all further distance calculations. Equidistant, equiangular radial lines ($n = 120$) were drawn around the edge-detected interface and the mean vector was calculated for each image. The average integrals of the ‘mean intensity versus distance from probe site’ vectors for all images were also used in comparing coated and control conditions.

ED-1 response was characterized by calculating the total intensity of each image. Since ED-1 fluorescent intensity was primarily localized to the region directly surrounding the probe site, total fluorescent intensity reflected the degree of macrophage reaction close to the probe–tissue interface. Therefore, a decrease in ED-1 intensity would indicate a lower number of macrophages and activated microglia at the probe–tissue interface.

Our objectives in analyzing the NeuN images were to quantify the number of neuronal nuclei and their proximity to the probe–tissue interface (figure 2(C)). RGB images were first converted to black and white. The area and centroid position of each contiguous white region was then calculated, where white regions represented cell bodies. Contiguous white regions with an area less than two standard deviations from the mean area were excluded from further analysis. Four endpoints were manually selected at the four corners of the remaining hole left after removal of the probe. From these four endpoints two lines were calculated which outlined the longest edges of the probe–tissue interface. White contiguous regions with centroids located less than or equal to $200 \mu\text{m}$ perpendicular to the drawn interface lines were included in further processing. The following features were stored for further analysis: distance to nearest centroid, total number of centroids, mean perpendicular distance of probe–tissue interface to centroids, and density (no. of centroids/area).

All statistical inferences were made between coated and uncoated conditions using Student’s *t*-test analysis (two-tailed) between like parameters. A minimum of four sections per cortical region was used to obtain the average for a particular marker.

2.7. *In vitro* primary microglial culture

To examine the response of microglia to the LN coating, *in vitro* microglial cell culture was studied. Primary mixed glial cell cultures were prepared from brains of newborn

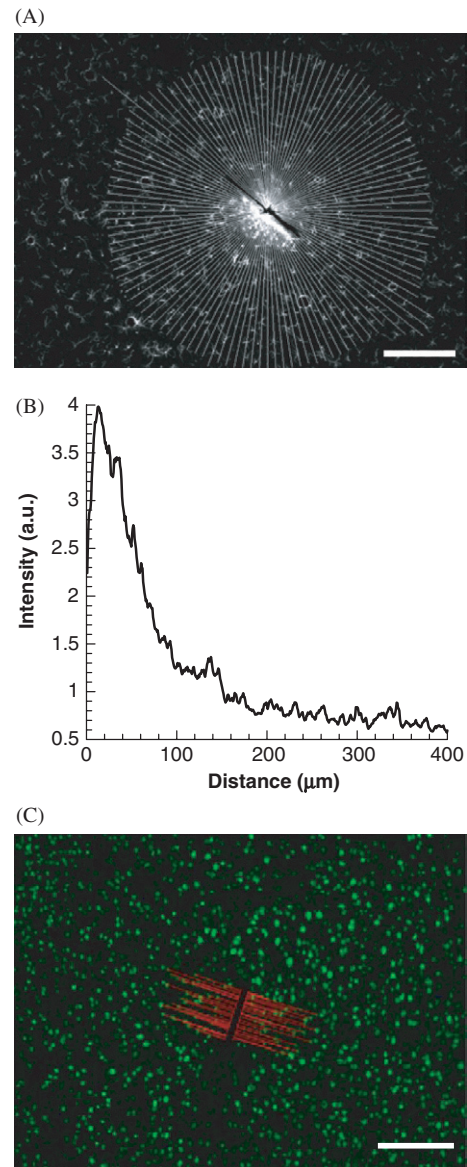


Figure 2. (A) Representative black and white sample image immunostained for GFAP with sampling lines ($n = 120$). Scale bar = $200 \mu\text{m}$. (B) Average fluorescent intensity profile plotted as a function of distance from the probe site. The area under the curve is the average total GFAP intensity. (C) Representative sample image immunostained for NeuN with probe site and distances to neuron centroid locations outlined in red. Scale bar = $200 \mu\text{m}$.

Sprague-Dawley rats on postnatal day 1 or day 2 as described by Giulian and Baker [25]. Briefly, the cerebral cortices of the animals were isolated aseptically and the meninges were carefully removed. The cleaned cortices were placed in a droplet of L15 medium (GIBCO) and mechanically dissociated using a fine dissecting knife. The tissue was further dissociated in 0.25% trypsin-EDTA (Invitrogen) at 37°C for 20 min. Following digestion, an equal volume of DMEM-F12 medium (GIBCO) with 10% fetal bovine serum was added to stop the reaction. After a brief centrifugation, the cells were resuspended and plated in 75 cm^2 tissue culture

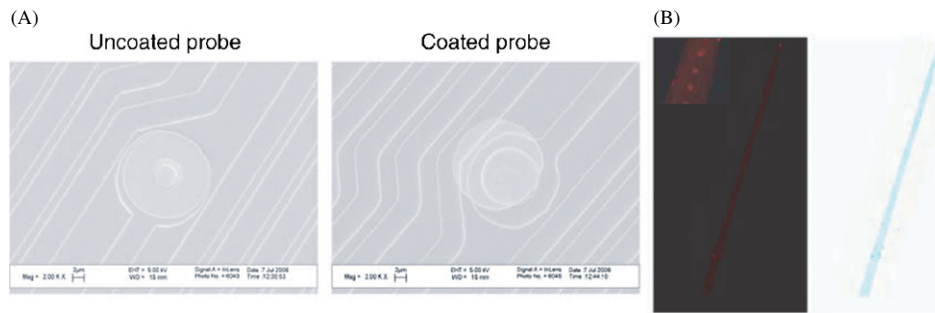


Figure 3. (A) SEM images of the uncoated and coated probes. Scale bar in the images is 2 μm . (B) Montage image of LN staining on probe that was subjected to insertion test. The inset is a higher magnification image showing detail of the recording sites. To aid in visualization, the corresponding pseudocolor image is shown.

Table 1. Oligonucleotide primers and optimal condition for real-time RT-PCR.

Cytokine	Size (bp)	Primers	Optimal condition		Accession number
			T_m ($^{\circ}\text{C}$)	MgCl_2 (mM)	
TNF- α F (5')	76	TGCCTCAGCCTCTTCTCATT	60.5	1.5	NM.012675
TNF- α R (5')		CAATCACCCCGAAGTTCAGT			
IL-1 F (5')	103	TGAAGAAGAGACGGCTAAGTTTC	55.0	1.5	NM.017019
IL-1 R (5')		TGAGGTGCTGATCTGGGTTG			
IL-6 F (5')	162	CCACCAGGAACGAAAAGTC	55.0	1.5	NM.012589
IL-6 R (5')		GGTATCCTCTGTGAAGTCGT			

flasks (Fisher) coated with poly-L-lysine at a density of one brain per flask in culture medium consisting of DMEM-F12 media supplemented with 10% fetal bovine serum and 1% penicillin/streptomycin. After 7–10 days, flasks were lightly shaken and the medium containing detached microglial cells were collected and centrifuged into a pellet. The cells were resuspended in DMEM-F12 medium with 10% fetal bovine serum, counted, and plated at a density of 150 000 cells cm^{-2} on sterile LN-coated and uncoated 1 \times 1 cm Si wafers, which were placed in individual wells of a 24-well culture plate and cultured for 24 h in 5% CO_2 atmosphere at 37 $^{\circ}\text{C}$.

2.8. Real-time PCR

The relative expressions of the targeted genes from the above microglial culture were measured using reverse-transcription ‘real-time’ quantitative polymerase chain reaction (RT-qPCR). The mRNA extraction was carried out using the materials and protocol provided in the RNeasy Mini Kit (Qiagen). Total RNA concentration and purity were determined by spectrophotometry at 260 and 280 nm. After isolation, the mRNA (0.5 μg) of each sample was reverse-transcribed with 20 μl of iScriptTM cDNA Synthesis Kit (Bio-Rad) containing random hexamer primers, oligo-(dT) and reverse transcriptase. The cDNA products were stored at -20°C or used immediately for PCR.

Real-time RT-PCR reactions were performed under each cytokine-specific condition to amplify three kinds of inflammatory cytokines, tumor necrosis factor alpha (TNF- α), interleukin-1 (IL-1) and interleukin-6 (IL-6) (table 1). These cytokines were chosen based on the compelling evidence of the

pivotal roles they play in influencing CNS response to injury [26]. For each of the primer sets, nonspecific amplification was confirmed absent after electrophoresis and ethidium bromide staining of agarose gels. PCR was carried out using the QuantiTect SYBR Green RT-PCR Kit and protocol. All RT-PCR experiments were performed using the iCycler (Bio-Rad). The protocol utilizes the following thermal parameters: activation step, 3 min at 95 $^{\circ}\text{C}$; three-step cycling (35 cycles): denaturation, 30 s at 95 $^{\circ}\text{C}$, annealing, 30 s at either 60.5 $^{\circ}\text{C}$ (TNF- α) or 55 $^{\circ}\text{C}$ (IL-1 and IL-6), extension, 1 min at 72 $^{\circ}\text{C}$. A melt curve was subsequently performed to confirm that there was no primer dimer in the PCR products, which began at 55 $^{\circ}\text{C}$ and increased to 95 $^{\circ}\text{C}$ in 0.4 $^{\circ}\text{C}$ increments. Relative standard curves for the candidate genes were performed each time the genes were analyzed and used for all the samples to obtain the relative quantity from the RT-qPCR of the targeted gene expression of each sample.

3. Results

3.1. Surface characterization and coating integrity

SEM was used to examine the surface of the LN-coated probe. As shown in figure 3(A), little difference was observed between surfaces of uncoated and coated probes. The surface appeared to be smooth and the coating was homogeneous, both on and around the recording site. A common concern with coating is the risk of delamination upon device insertion. Using an antibody against LN, we evaluated the coating integrity after the probe was subjected to insertion process. LN-positive antibody binding was observed along the shank

and on the recording sites (figure 3(B)), suggesting that the insertion step did not disrupt the distribution of the coating on the probe surface.

3.2. ED-1 immunoreactivity

Activated microglia and macrophages were identified via ED-1 staining. One day after surgery, the uncoated probe site was characterized by a faint diffusive ED-1 staining with a few labeled cells (figure 4). On the coated probe site, the staining showed a significant increase in the number of small, amoeboid ED-1 positive cells surrounding the area. The intensity of the ED-1 staining for the coated probe was ~60% higher than that of the uncoated probe ($p < 0.05$).

One week after insertion, the responses were very similar between the uncoated and coated probes (figure 4). The majority of the ED-1+ cells had the appearance of large, round, blood-borne monocytes/macrophages. Smaller, process-bearing microglia were also seen at various distances from the injury site. However, differences in ED-1 staining were seen 4 weeks post-surgery. Lower ED-1+ staining was observed for the coated probe: ~20% less than that of the uncoated probe ($p < 0.05$). The ED-1+ cell layer was more compact (shown by the arrow) in contrast to the observation of 1 week, and only phagocytic amoeboid microglia/macrophage cells were seen around the insertion site.

3.3. GFAP immunoreactivity

GFAP is a commonly used marker to evaluate reactive gliosis as an astrocytic reaction to injury. One day after surgery, both coated and control insertion sites were characterized by appearance of elevation in GFAP intensity (figure 5(A)), compared to the normal cortical tissue far away from the insertion site. Such elevation was observed up to 400 μm from the site.

After 1 week, in both control and LN-coated cases, the insertion sites showed a substantial increase in GFAP reactivity (figure 5(A)). The staining revealed astrocytes surrounding the insertion sites became hypertrophic, elongated with thick processes as compared to those in the intact brain region, which were more stellate in appearance. GFAP immunoreactivity was maximum in the immediate border zones of the insertion site and declined progressively as a function of distance from the site, extending up to 300 μm on either side. There was little difference in terms of GFAP intensity between the coated probe and uncoated probe at the 1 day and 1 week post-implantation, as demonstrated by the average intensity line profile (figures 5(B) and (C)).

By week 4, the GFAP positive zone became compact around the uncoated probe insertion site, approximately 100 μm in radius (figure 5(A)). These astrocytes exhibited an interwoven appearance. For the coated probe, the GFAP intensity within the vicinity of the insertion site decreased even more dramatically and was comparable to that in the intact region. The average intensity line profiles indicated a significant GFAP reduction for the coated probe (~50% less than the uncoated probe ($p < 0.01$), figures 5(B) and (C)).

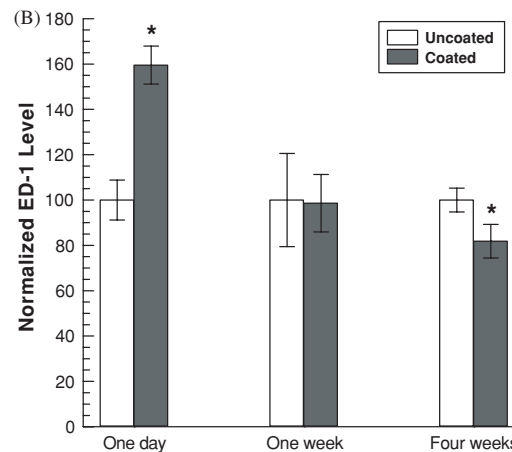
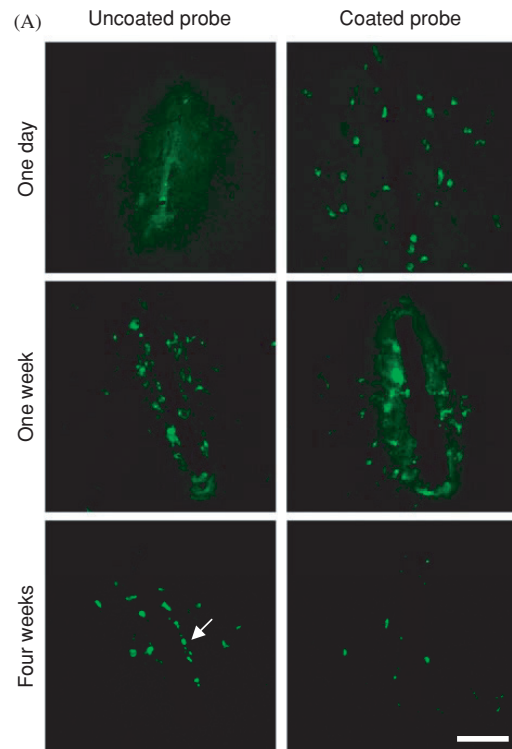


Figure 4. (A) Representative images of ED-1 staining for both uncoated and coated conditions at 1 day, 1 week and 4 weeks post-insertion. (B) The percentage of ED-1 fluorescent intensity of coated compared to uncoated was plotted. At day one, the coated probe showed significantly higher ED-1 intensity than the uncoated probe ($p < 0.05$). No significant difference was observed between conditions at the 1 week time point. Intensity was significantly reduced for coated probes at the 4 week time point ($p < 0.05$). Scale bar = 50 μm .

3.4. Immunostaining of neurons

Neuronal response to the probes was characterized via NeuN staining (figure 6), which is specific to neuronal nuclei. One day post-surgery, a decrease in the number of neurons immediately adjacent to the insertion site was observed for both the uncoated and coated probes. By the end of 1 week, a neuron-depleted zone approximately 30 μm away from

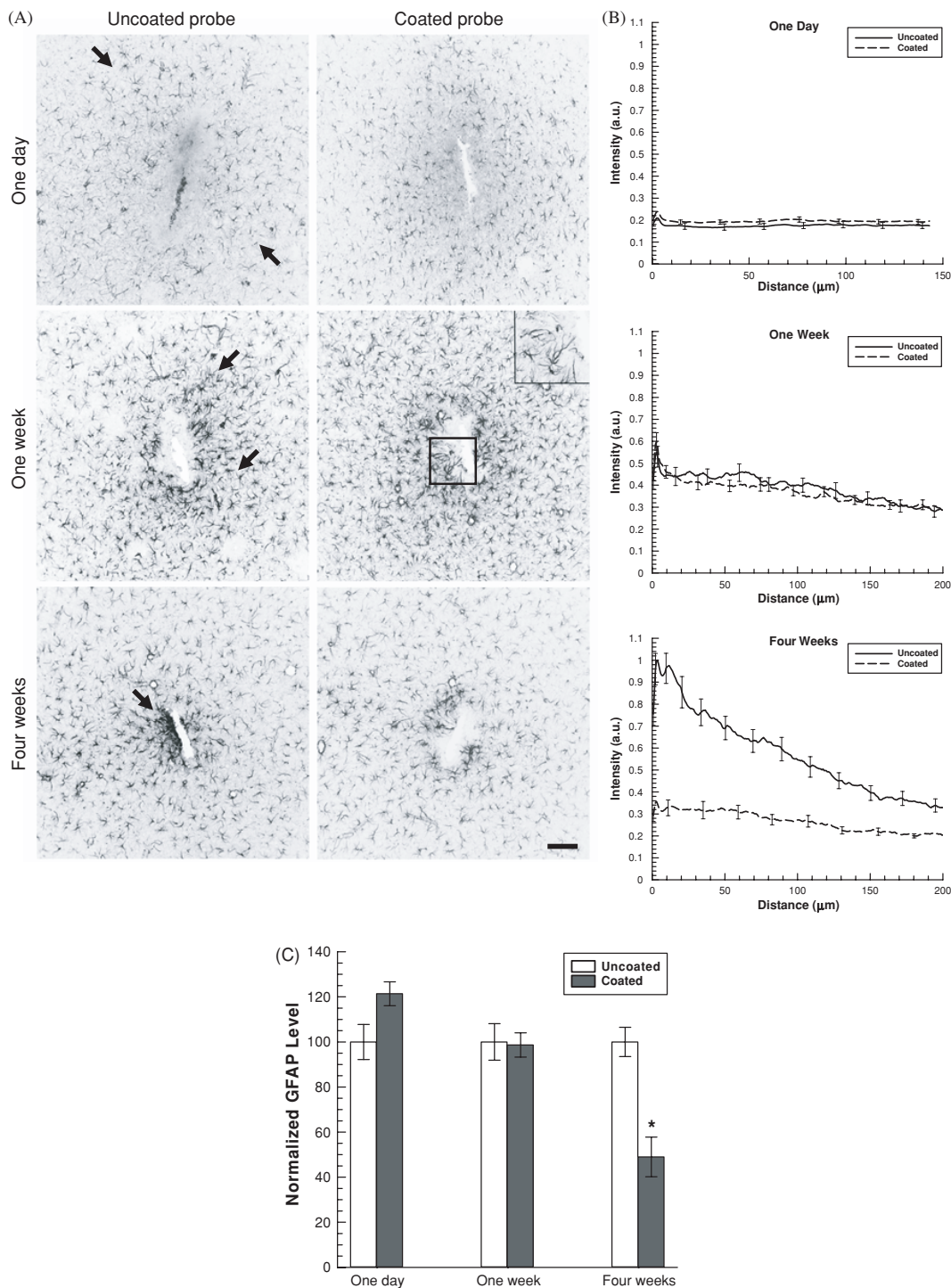


Figure 5. (A) GFAP immunohistochemistry of tissue sections from brains implanted with uncoated probes and LN-coated probes at 1 day, 1 week and 4 weeks post-insertion. One day after surgery, elevation of GFAP intensity started to emerge surrounding the insertion site (see arrows). By 1 week post-surgery, hypertrophic astrocytes with intense GFAP labeling were observed around probe sites (see inset and arrows). The response was similar between the uncoated and coated probes. However, by week four, a less intense GFAP staining was located around the coated probe site in comparison to the uncoated probe site, where a compact astrocytic sheath had formed (see arrow). (B) Quantitative comparison of GFAP immunoreactivity between the uncoated and coated probes was made via GFAP intensity profiles as a function of distance from the probe site. SEM bars from 20% of the data points were displayed. (C) Total GFAP intensity for the coated probe, defined as the integral of each intensity line profile shown in (B), was normalized to that of the uncoated probe. As shown in the plots, no statistical difference in the mean fluorescent intensity profile was observed at the 1 day and 1 week time points. At the 4 week time point, GFAP intensity was higher for uncoated than coated ($p < 0.01$); in other words, the percentage of coated GFAP fluorescent intensity compared to uncoated was significantly reduced ($p < 0.01$). Scale bar = 100 μm.

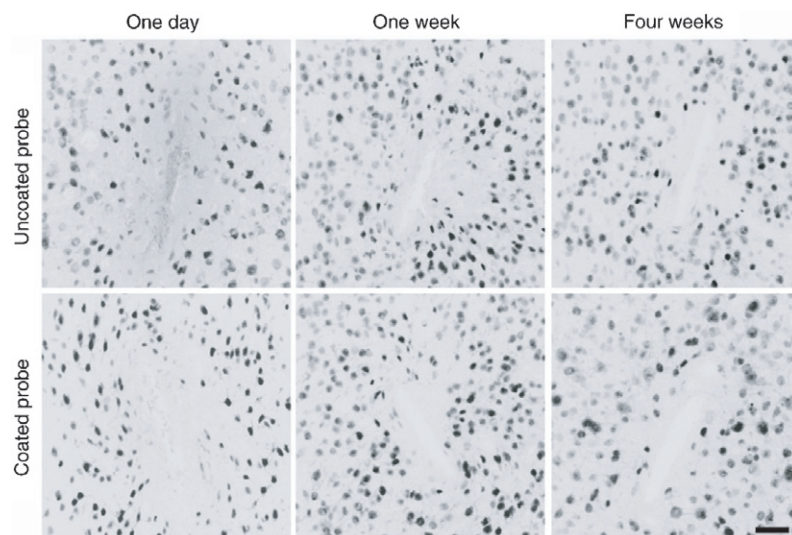


Figure 6. Immunostaining of neurons with NeuN at 1 day, 1 week and 4 weeks post-insertion. The distribution of NeuN positive cells around the probe site was similar for both probes at all three time points. Scale bar = 50 μm .

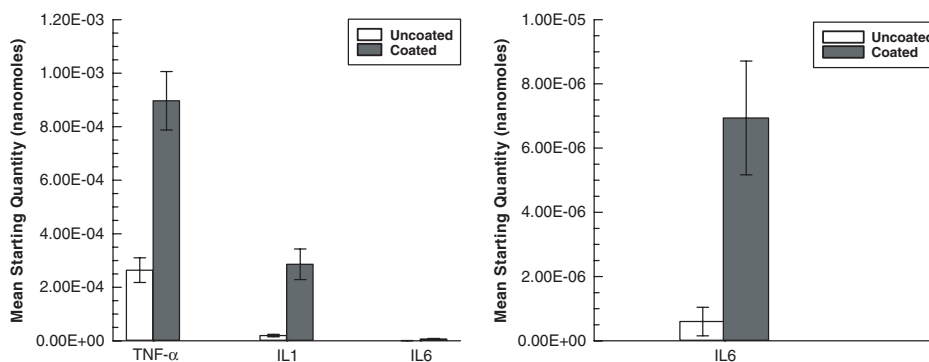


Figure 7. Gene expression of pro-inflammatory cytokines TNF- α , IL-1 and IL-6 after 24 h microglial culture quantified by real-time RT-PCR. There was statistic difference for each gene between microglia grown on the bare Si and on LN-coated Si ($p < 0.01$).

the probe site was developed for both uncoated and coated probes. At the end of 4 weeks, little change was seen for the zone. NeuN quantitative analysis did not reveal any statistical differences between coated and uncoated conditions. This was the case in all of the parameters we investigated, including distance to nearest neuron, total number of neurons, mean perpendicular distance of probe–tissue interface to neurons, and density (no. of neurons/area). This may imply that a coating employing a diffusible pharmacological agent, e.g. nerve growth factor, is necessary to modulate neurons beyond the glial scar.

3.5. Real-time PCR

Real-time RT-PCR analysis of cytokine production indicated that there were significant, quantitative differences in microglial responses to bare silicon and LN-coated silicon samples (figure 7). Overall, the pro-inflammatory cytokine expression was significantly higher ($p < 0.01$) for microglia cultured on the LN-coated silicon sample. Cells had a more

than three-fold increase in TNF- α expression, 14-fold increase in IL-1 expression, and 11-fold increase in IL-6 expression. Regardless of the substrate type, TNF- α expression was higher than IL-1, and IL-6 expression was lowest.

4. Discussion

The main objective of this study was to evaluate *in vivo* brain tissue response to micromachined Si neural probes modified with nanoscale coating of LN. Several studies have investigated CNS response to LN *in vitro* including isolated neurons [27], neurons and astrocytes in co-culture [28], and microglia [29]. However, the effect of LN on microglia/macrophage and astrocyte function *in vivo*, to our knowledge, has not been explored. In this study, local presence of neurons, macrophages/activated microglia and reactive astrocytes at the implantation site of Si probes were compared between bare and LN-coated probes 1 day, 1 week and 4 weeks post-implantation.

Studies have shown that following a penetrating injury to the central nervous system (CNS), a complex cellular event occurs which usually leads to reactive gliosis [30, 31]. Given the high vascular density in the brain, inserting the micromachined silicon probe into the brain inevitably ruptures blood vessels. Recently, Bjornsson *et al* [32] have demonstrated the vascular damage generated by the neuroprosthetic device insertion. As a result of vascular damage, macrophages derived from the bloodstream are recruited to the injury site and microglia, the resident immune cell of the brain, become activated. One indication of microglial activation is their transformation in morphology from ramified to amoeboid configuration [33]. In our study, ED-1+ microglia/macrophages were observed immediately next to the insertion site, indicating that these cells form the front line of defense against the implanted probes. Although little difference between LN-coated and uncoated probes was observed in microglia/macrophage response after 1 week, differences were noted in both the earlier acute phase (1 day) and later chronic phase (4 weeks). The coated probe induced a considerably higher ED-1 staining at 1 day post-implantation, suggesting that the LN coating initiated a greater response from microglia/macrophages. *In vitro* real-time PCR results have shown that microglia cultured on the LN surface had substantial upregulation of pro-inflammatory cytokines, namely, TNF- α , IL-1 and IL-6 mRNA expression. Our observation of microglia activation by LN is consistent with the observation of Chamak and Mallat [29]. Studies have shown that these pro-inflammatory cytokines secreted by activated microglia can further activate adjacent microglia and astrocytes, via autocrine and paracrine pathways, leading to propagation and enhancement of the acute inflammatory response [34, 35]. These findings suggest that LN may have an acute stimulatory effect on microglia, which is further supported by the observed higher ED-1 response for coated probes after 1 day. Significantly lower ED-1 staining observed after 4 weeks for the coated probe implies that the coating evoked less microglia activation in the long term.

One possible mechanism for the beneficial attenuation in astrogliosis at 4 weeks with LN-coated probes is that LN triggers a boosted, well-coordinated, clean-up response from microglia/macrophages of the necrotic debris after injury. Mitigation of astrogliosis by activation of microglia/macrophages is supported by several relevant studies. Using a microlesion model which resulted in minimal necrotic debris, Davies *et al* reported that amoeboid microglia appeared 1 day after injury and quickly disappeared [36]. The disappearance of microglia was likely due to their successful removal of the debris resulting from the microlesions. Schwartz *et al* have investigated treatment strategies for tissue repair in the injured spinal cord using the approach of stimulating, as opposed to suppressing, the CNS immune system through activated macrophages [37–39].

Besides microglia, astrocytes play an important role in response to injury. In our study, the response patterns of astrocytes to injury caused by probe insertion were qualitatively comparable to that observed by Szarowski *et al* [12]. Initially, a broad zone of reactive astrocytes,

characterized by their larger size, longer and thicker processes, and increased GFAP expression, surrounded both uncoated and LN-coated probe insertion sites. This broad band of reactive astrocytes indicated that astrocytes started to form a barrier between the injury site and the surrounding tissue. After 4 weeks post-implantation, the zone had evolved into a narrow sheath of tightly interwoven astrocyte layer encircling the uncoated probe. In contrast, a mild astrocytic response, as characterized by disconnected segments of relatively low GFAP expression, was seen after 4 weeks for the coated probe.

The observed correlation between ED-1 immunoreactivity and GFAP immunoreactivity chronically is interesting as it indicates intercellular crosstalk between microglia/macrophages and astrocytes. As mentioned above, upon activation, microglia release cytokine products, such as IL-1, IL-6 and TNF- α , which can mediate astrogliosis [34]. It is possible that the diminished astrocytic response for the coated probe in the chronic phase resulted from the reduced number of activated microglia present at the injury site, which induced a lower cytokine production. The lack of difference in astrocyte response 1 day following surgery between the uncoated and coated probes may be due to a sub-threshold concentration of the produced cytokines required for astrocyte activation *in vivo* at this time point.

The high-density cellular sheath surrounding Si MEAs has been suggested as being a significant cause in the electrical isolation of implants in the brain [13]. At least three hypotheses for how the glial scar degrades signal quality over time have been proposed: (1) by promoting a chemically inhibitory environment for neural processes [30], (2) by increasing the distance between recording site and nearest neurons [40], and (3) by insulating the probe from surrounding neurons, thus increasing impedance [13, 30].

Neuronal proximity to electrode recording sites, neuronal density, and current flow between neurons and electrode sites are three primary factors affecting recording quality. Differences in neuronal proximity to electrode recording site and neuronal density between bare and LN-coated probes were not observed. This finding sheds light on the cellular audience of immobilized and diffusion-based coating strategies. A coating based on protein/drug immobilization to the electrode surface is perhaps not well suited for targeting neurons, since the cellular layers of microglia and reactive astrocytes separate neurons from ‘seeing’ the electrode surface. A coating based on the diffusion of a pharmacological agent(s) might be a better method to influence neurons beyond the glial scar. While a diffusion-based coating has the potential for modulating neuronal and glial cells, immobilized coatings affect those cells in contact with the electrode surface, namely, microglia and astrocytes. Although neuron-to-recording site distance is a critical factor in neural recordings, it is not sufficient. It has been suggested that glial cells are a major cause of these phenomena by obstructing pathways for current flow between neurons and recording sites [41]. It follows that a tightly woven glial sheath between electrode and neuron would block any low resistance paths between recording site and nearby neurons. This line of reasoning is supported by a study reporting that regions in and around glial scar have less permissible

diffusion [42]. As with molecules, glial scars impede current flow between electrodes and nearby neurons by a combination of a decrease in extracellular fluid volume between astrocytes and an increase in resistivity due to the tissue composition itself [43]. The intimate relationship between extracellular fluid volume and electrode impedance has been studied in the cochlea [44]. A mitigated glial scar with extracellular clefts between astrocytes may significantly improve recording reliability by sustaining low resistance channels for current flow between firing neurons and recording sites. Since a complete analysis of chronic recording data was beyond the scope of this study, we are at this time unable to correlate our histological results to recording quality over time.

In summary, the surface modification of Si MEAs with PEI-LN LbL coating is able to mitigate the long-term tissue response to chronic implants. Long-term reduction of glial scar surrounding the coated implant was correlated with an initial amplified local activation of resident and blood-borne macrophages induced by LN. These findings suggest that LN may be useful in mitigating astrogliosis in other neural-related chronic applications as well. We suggest that the addition of diffusible neurotrophic factors may further facilitate the active 'management' of the interface to promote long-term recording stability.

Acknowledgments

The authors gratefully acknowledge the contributions of Mr Matt Davis, Dr Young-tae Kim and Dr Rupal Thazhath for their technical assistance. Funding support was provided by the National Institute of Health, R01 DC06849 and NS45072 (RVB). GTEC, an NSF funded ERC located at Georgia Institute of Technology and Emory University, is also acknowledged for the use of core facilities.

References

- [1] Bell T E, Wise K D and Anderson D J 1998 A flexible micromachined electrode array for a cochlear prosthesis *Sensors Actuators A* **66** 63–9
- [2] Rauschecker J P and Shannon R V 2002 Sending sound to the brain *Science* **295** 1025–9
- [3] Breit S, Schulz J B and Benabid A L 2004 Deep brain stimulation *Cell Tissue Res.* **318** 275–88
- [4] Lozano A M, Dostrovsky J, Chen R and Ashby P 2002 Deep brain stimulation for Parkinson's disease: disrupting the disruption *Lancet Neurol.* **1** 225–31
- [5] Piper M, Abrams G M and Marks W J Jr 2005 Deep brain stimulation for the treatment of Parkinson's disease: overview and impact on gait and mobility *NeuroRehabilitation* **20** 223–32
- [6] Hetke J F and Anderson D J 2002 Silicon microelectrodes for extracellular recording *Handbook of Neuroprosthetic Methods* ed W E Finn and P G LoPresti (Boca Raton, FL: CRC Press)
- [7] Hochberg L R, Serruya M D, Friehe G M, Mukand J A, Saleh M, Caplan A H, Branner A, Chen D, Penn R D and Donoghue J P 2006 Neuronal ensemble control of prosthetic devices by a human with tetraplegia *Nature* **442** 164–71
- [8] Kipke D R, Vetter R J, Williams J C and Hetke J F 2003 Silicon-substrate intracortical microelectrode arrays for long-term recording of neuronal spike activity in cerebral cortex *IEEE Trans. Neural Syst. Rehabil. Eng.* **11** 151–5
- [9] Branner A, Stein R B and Normann R A 2001 Selective stimulation of cat sciatic nerve using an array of varying-length microelectrodes *J. Neurophysiol.* **85** 1585–94
- [10] Rutten W L C, van Wier H and Put J M H 1991 Sensitivity and selectivity of intraneural stimulation using a silicon electrode array *IEEE Trans. Biomed. Eng.* **38** 192–8
- [11] Editorial 2006 Is this the bionic man? *Nature* **442** 109
- [12] Szarowski D H, Andersen M D, Retterer S, Spence A J, Isaacson M, Craighead H G, Turner J N and Shain W 2003 Brain response to micro-machined silicon devices *Brain Res.* **983** 23–35
- [13] Turner J N, Shain W G, Szarowski D H, Andersen M D, Martins S, Isaacson M and Craighead H G 1999 Cerebral astrocyte response to micro-machined silicon implants *Exp. Neurol.* **156** 33–49
- [14] Biran R, Martin D C and Tresco P A 2005 Neuronal cell loss accompanies the brain tissue response to chronically implanted silicon microelectrode arrays *Exp. Neurol.* **195** 115–26
- [15] Edell D J, Toi V V, McNeil V M and Clark L D 1992 Factors influencing the biocompatibility of insertable silicon microshafts in cerebral cortex *IEEE Trans. Biomed. Eng.* **39** 635–43
- [16] Polikov V S, Tresco P A and Reichert W M 2005 Response of brain tissue to chronically implanted neural electrodes *J. Neurosci. Methods* **148** 1–18
- [17] Cui X, Lee V A, Raphael Y, Wiler J A, Hetke J F, Anderson D J and Martin D C 2001 Surface modification of neural recording electrodes with conducting polymer/biomolecules blends *J. Biomed. Mater. Res.* **56** 261–72
- [18] Cui X, Wiler J, Dzaman M, Altschuler R A and Martin D C 2003 In vivo studies of polypyrrole/peptide coated neural probes *Biomaterials* **24** 777–87
- [19] Massia S P, Holecko M M and Ehteshami G R 2003 In vitro assessment of bioactive coatings for neural implant applications *J. Biomed. Mater. Res.* **68A** 177–86
- [20] James C D, Davis R C, Kam L, Craighead H G, Isaacson M, Turner J N and Shain W 1998 Patterned protein layers on solid substrates by thin stamp microcontact printing *Langmuir* **14** 741–4
- [21] He W and Bellamkonda R V 2005 Nanoscale neurointegrative coatings for neural implants *Biomaterials* **26** 2983–90
- [22] Griffith R W and Humphrey D R 2006 Long-term gliosis around chronically implanted platinum electrodes in the Rhesus macaque motor cortex *Neurosci. Lett.* **406** 81–6
- [23] Reprinted from Paxinos G and Watson C 1997 *The Rat Brain in Stereotaxic Coordinates* (San Diego, CA: Academic)
- [24] Kim Y, Hitchcock R W, Bridge M J and Tresco P A 2004 Chronic response of adult rat brain tissue to implants anchored to the skull *Biomaterials* **25** 2229–37
- [25] Giulian D and Baker T J 1986 Characterization of ameboid microglia isolated from developing mammalian brain *J. Neurosci.* **6** 2163–78
- [26] John G R, Lee S C and Brosnan C F 2003 Cytokines: powerful regulators of glial cell activation *Neuroscientist* **9** 10–22
- [27] Ignatius M J, Sawhney N, Gupta A, Thibadeau B M, Monteiro O R and Brown I G 1998 Bioactive surface coatings for nanoscale instruments: effects on CNS neurons *J. Biomed. Mater. Res.* **40** 264–74
- [28] Costa S, Planchenault T, Charriere-Bertrand C, Mouchel Y, Fages C, Juliano S, Lefrancois T, Barlovatz-Meimon G and Tardy M 2002 Astroglial permissivity for neuritic outgrowth in neuron-astrocyte cocultures depends on regulation of laminin bioavailability *Glia* **37** 105–13
- [29] Chamak B and Mallat M 1991 Fibronectin and laminin regulate the in vitro differentiation of microglial cells *Neuroscience* **45** 513–27

- [30] Fawcett J W and Asher R A 1999 The glial scar and central nervous system *Brain Res. Bull.* **49** 377–91
- [31] Silver J and Miller J H 2004 Regeneration beyond the glial scar *Nat. Rev. Neurosci.* **5** 146–56
- [32] Bjornsson C S, Oh S J, Al-Kofahi Y A, Lim Y J, Smith K L, Turner J N, De S, Roysam B, Shain W and Kim S J 2006 Effects of insertion conditions on tissue strain and vascular damage during neuroprosthetic device insertion *J. Neural Eng.* **3** 196–207
- [33] Kreutzberg G W 1996 Microglia: a sensor for pathological events in the CNS *Trends Neurosci.* **19** 312–8
- [34] Hanisch U 2002 Microglia as a source and target of cytokines *Glia* **40** 140–55
- [35] Kyrkanides S, O'Banion M K, Whiteley P E, Daeschner J C and Olschowka J A 2001 Enhanced glial activation and expression of specific CNS inflammation-related molecules in aged versus young rats following cortical stab injury *J. Neuroimmunol.* **119** 269–77
- [36] Davies S J, Field P M and Raisman G 1996 Regeneration of cut adult axons fails even in the presence of continuous aligned glial pathways *Exp. Neurol.* **142** 203–16
- [37] Lazarov-Spiegler O, Solomon A S, Zeev-Brann A B, Hirschberg D L, Lavie V and Schwartz M 1996 Transplantation of activated macrophages overcomes central nervous system regrowth failure *FASEB J.* **10** 1296–302
- [38] Lazarov-Spiegler O, Rapalino O, Agranov G and Schwartz M 1998 Restricted inflammatory reaction in the CNS: a key impediment to axonal regeneration? *Mol. Med. Today* **4** 337–42
- [39] Zeev-Brann A B, Lazarov-Spiegler O, Brenner T and Schwartz M 1998 Differential effects of central and peripheral nerves on macrophages and microglia *Glia* **23** 181–90
- [40] Liu X, McCreery D B, Carter R R, Bullara L A, Yuen T G H and Agnew W F 1999 Stability of the interface between neural tissue and chronically implanted intracortical microelectrodes *IEEE Trans. Rehabil. Eng.* **7** 315–26
- [41] Robinson D A 1968 The electrical properties of metal microelectrodes *Proc. IEEE* **56** 1065–71
- [42] Roitbak T and Sykova E 1999 Diffusion barriers evoked in the rat cortex by reactive astrogliosis *Glia* **28** 40–8
- [43] Grill W M and Mortimer J T 1994 Electrical properties of implant encapsulation tissue *Ann. Biomed. Eng.* **22** 23–33
- [44] Duan Y Y, Clark G M and Cowan R S C 2004 A study of intra-cochlear electrodes and tissue interface by electrochemical impedance methods *in vivo Biomaterials* **25** 3813–28